Journal of ELECTRONIC MATERIALS, Vol. 46, No. 7, 2017
DOI: 10.1007/s11664-017-5353-8
© 2017 The Minerals, Metals & Materials Society

Effect of Co^{2+} Ions Doping on the Structural and Optical Properties of Magnesium Aluminate

KIRAN KANWAL,[1] BUSHRA ISMAIL,[2] K.S. RAJANI,[3] N.J. SUTHAN KISSINGER,[4] and AURANG ZEB[4,5]

1.—Nano Physics Laboratory, Department of Applied Physics, Federal Urdu University of Arts, Science and Technology, Islamabad, Pakistan. 2.—COMSATS Institute of Information Technology, Abbottabad, Pakistan. 3.—Department of Physics, School of Engineering, Amritha University, Coimbatore, India. 4.—Department of General Studies, Physics Group, Jubail University College, Royal Commission in Jubail, Jubail Industrial City 31961, Saudi Arabia. 5.—e-mail: aurangzebbabar@yahoo.com

Cobalt-doped nanosized magnesium aluminate ($Mg_{1-x}Co_xAl_2O_4$) samples having different compositions (x = 0.2, 0.4, 0.6, 0.8, 1.0) were synthesized by a chemical co-precipitation method. All samples were characterized by means of x-ray diffraction (XRD), scanning electron microscopy, Fourier transform infrared spectroscopy, ultra violet–visible spectroscopy, photoluminescence and diffused reflectance spectroscopy. The results of XRD revealed that the samples were spinel single phase cubic close packed crystalline materials. The lattice constant and x-ray density were found to be affected by the ionic radii of the doped metal cations. Using the Debye–Scherrer formula, the calculated crystalline size was found to be Co^{2+} ion concentration-dependent and varied between 32 nm and 40 nm. Nano-dimensions and phase of the $Mg_{1-x}Co_xAl_2O_4$ samples were analyzed and the replacement of Mg^{2+} ions with Co^{2+} ions was confirmed by elemental analysis. Three strong absorption bands at 540 nm, 580 nm and 630 nm were observed for the doped samples which are attributed to the three spin-allowed $^4T_{1g}$ (^4F) $\rightarrow$ $^4T_{2g}$, $^4A_{2g}$, $^4T_{1g}$ (4P) electronic transitions of Co^{2+} at tetrahedral lattice sites. Nanophosphors have optical properties different from bulk because of spatial confinement and non-radiative relaxation. Decreases in particle size can increase the surface area and the defects, which can in turn increase the luminescent efficiency to make it very useful for tunable laser operations, persistent phosphorescence, color centers, photoconductivity and luminescence for display technology. $MgAl_2O_4$ was doped with Co^{2+} ions using a co-precipitation method and the optical absorption studies revealed that there is a decrease of band gap due to the increase of Co^{2+} content. The emission intensity of this phosphor is observed at 449 nm with a sharp peak attributed to the smaller size of the particles and the homogeneity of the powder.

Key words: Co^{2+} doping, nano-phosphor, photoluminescence, spinel

INTRODUCTION

Magnesium aluminate ($MgAl_2O_4$), an oxide mixture of alumina and magnesia, has several appealing properties.[1] It has a high melting point (2135°C) and a density that lies between MgO and Al_2O_3 oxides.[2] Its excellent mechanical strength at high temperatures makes it a good material for industrial applications such as ceramics and in technology, such as fusion reactors, humidity sensors, color displays and light-emitting diodes.[3]

$MgAl_2O_4$ has a high degree of cation disorder due to intermixing of Al^{3+} and Mg^{2+} ions, as it has two

(Received April 10, 2016; accepted February 3, 2017; published online February 24, 2017)

different types of site symmetries on which cations having charge symmetries A^{2+} and B^{3+} are found to be distributed. Tetrahedral symmetry sites number 64 iof which 8 sites are filled while only 16 aluminum ions with the charge state Al^{3+} are found among the 32 octahedral sites.[4] It has face-centered cubic structure with 8.08 Å lattice constant.[5]

High degrees of innate defects are responsible for the strange optical behavior of pure synthetic and natural spinel. These defects can be enhanced by various types of irradiations, like ultra violet (UV) rays or electrons. Employing the spinel cage with some kinds of impurities can also increase the defects for optical properties such as persistent phosphorescence, color centers, photoconductivity and luminescence.[6] Impurities can react with the vacancies and interstitials which results in the lowering of the efficiency of the recombination rate, making the survival of defects even better.

The luminescence properties of Co^{2+}-doped $MgAl_2O_4$ prepared by a co-precipitation method are investigated in the present work. The energy level diagram of Co^{2+} having T_d symmetry is similar to that of the O_d symmetry of Cr^{3+} ions, except for ligand field strength which is weaker for the Co^{2+} ions than for the Cr^{3+} ions. The luminescence properties at lower temperatures and in infrared regions have been investigated earlier but has been reported more recently in the visible regions in $LiGa_5O_8$.[7] A co-precipitation technique was employed for the synthesis of nanosized $MgAl_2O_4$ spinel, since the wet chemical synthesis processes require low processing temperatures,[8] and good control on particle size and morphology. The synthesis of cobalt-doped $MgAl_2O_4$ samples is based on the continuous isomorphy between MgO and CoO (Ionic radii of Mg^{2+} and Co^{2+} are very close), which facilitates the substitution of Mg^{2+} ions by Co^{2+} ions and the formation of $Mg_{1-x}Co_xAl_2O_4$ solid solutions.

EXPERIMENTAL PROCEDURE

Cobalt-doped $MgAl_2O_4$ samples, $Mg_{1-x}Co_xAl_2O_4$, were synthesized by co-precipitation method. Figure 1 shows the schematic representation of the various steps involved in the co-precipitation method used in the present study. Al $(NO_3)_3{\cdot}9H_2O$ (Merck, 95.0%), Mg $(NO_3)_2{\cdot}6H_2O$ (Merck, >99.99%) and Co $(NO_3)_2{\cdot}6H_2O$ (Sigma Aldrich, >99.99%) were the chemicals used for synthesis. An aqueous solution of metal nitrates was made by separately mixing stoichiometric amounts of nitrates into 100 ml of distilled water along with continuous stirring and heating at 60°C to form clear solutions. The solutions were added simultaneously into 200 ml of distilled water and 2 M ammonia solution was added dropwise into the clear solution to control pH up to 9. Stirring was necessary in order to maintain the homogeneity of the samples. The obtained viscous solution was aged overnight at room temperature. The precipitates formed were

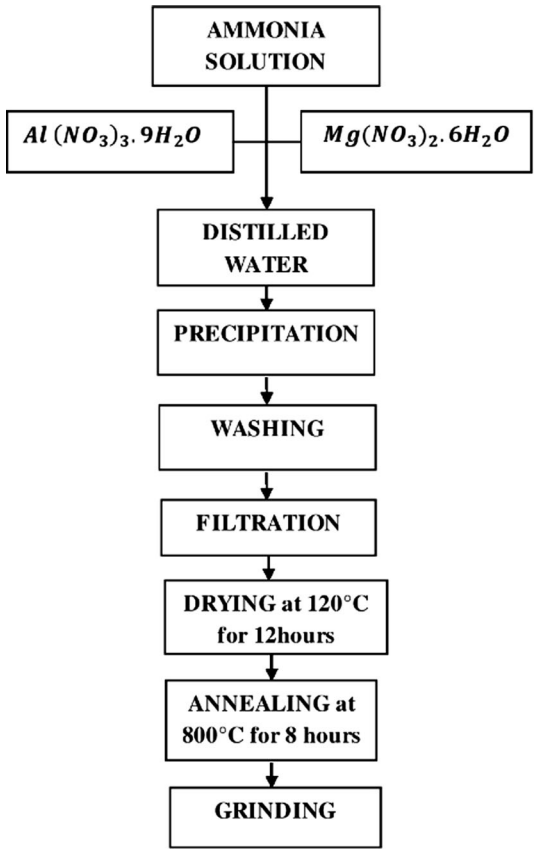

Fig. 1. Schematic diagram of the co-precipitation method used to prepare the $Mg_{1-x}Co_xAl_2O_4$ samples.

then washed several times with distilled water, filtered with filter paper and dried in an oven at 120°C for 12 h. The dried samples were annealed in the furnace at 800°C for 8 h and then ground to obtain nano-sized powder.

For investigating the different characteristics of the samples, various techniques were employed. The crystal structural parameters (lattice constant, density, volume and grain size) were measured by x-ray diffraction (XRD) data obtained by using an x-ray diffractometer (Philips X'pert PRO 3040/60). The data were obtained in the 2θ range (10°–80°) and the x-ray used was copper (Cu-Kα). The reference card used to index the pattern obtained from the $Mg_{1-x}Ni_xAl_2O_4$ samples was Inorganic Crystal Structure Database (ICSD) ref. code 00-021-1152, spinel, a = 8.08 Å, V_{cell} = 529 Å^3.[9] The morphology of the sample along with elemental analysis was studied using scanning electron microscopy (SEM) which was coupled with energy dispersive spectroscopy (EDS). Fourier transform infrared spectroscopy (FTIR) was carried out in the mid-infrared range (400–4000 cm^{-1}). An Excalibur Bio-Rad (FTS 3000M X) spectrometer was engaged to record the FTIR spectra. For optical analysis, diffuse reflectance spectroscopy (DRS), ultra violet–visible spectroscopy (UV–vis), and photoluminescence (PL)

analysis were used. DRS were used to find the diffused reflectance and band gap of the samples and the analysis was done with a Perkin-Elmer UV–vis Spectrometer Lambda 900 in the visible range (400–850 nm).

Absorption of the samples was studied by the support of UV–vis using a Perkin-Elmer UV–vis Spectrometer Lambda 25 in the visible region. PL measurements were performed in a spectrofluorimete (SPEX-Fluorolog 2) with a double-grating 0.22-m monochromator (SPEX 1680) and a 450-W Xenon lamp as the excitation source. All spectra were recorded using a detector mode correction. PL studies were carried out to find the emission wavelength of the samples in the visible region.

RESULTS AND DISCUSSION

X-ray Diffraction Analysis

Figure 2 shows the powder XRD patterns of the $Mg_{1-x}Co_xAl_2O_4$ samples. The crystallinity of the samples is noted by well-defined high intensity peaks having *hkl* values (220), (311), (400), (422), (511) and (440) which match well with the standard reference card (ICSD ref. code 00-021-1152, spinel) with a lattice constant a = 8.08 Å. The absence of an impurity peak confirms the single phase cubic structure of the spinel[10] and also has a significant effect on the specimen.

To investigate various structural parameters of synthesized sample by XRD the following relationships were used:

$$a = \sqrt{h^2 + k^2 + l^2} \times d_{hkl} \quad (1)$$

$$V_{\text{cell}} = a^3 \quad (2)$$

$$d_{\text{x-ray}} = \frac{Z \cdot M}{N_A V_{\text{cell}}} \quad (3)$$

$$D_s = \frac{K\lambda}{\beta \text{Cos}\theta} \quad (4)$$

where h^2, k^2, l^2 values are the squares of miller indices, Z indicates the number of molecules in the formula unit (8 for spinel as it is cubic), a is the crystallite size, $d_{\text{x-ray}}$ is the density, M indicates the molar mass, N_A is the Avogadro number (6.02×10^{23}/mole), and V_{cell} is the unit cell volume. D_s, the crystallite size, can be calculated by the Scherrer formula given in Eq. 4. In this equation, K is the constant which has a value 0.9 λ. The wavelength, λ, of incident x-rays has a value equal to 1.542 Å, β is the full width of the diffracted line at half maximum, and θ is the Bragg's angle.

The various lattice parameters for the $Mg_{1-x}Co_xAl_2O_4$ samples with different x contents (x = 0.2, 0.4, 0.6, 0.8, 1.0) were calculated using Eqs. 1, 2, 3, and 4 and are tabulated in Table I. The lattice constant of the sample was calculated from Eq. 1, in which

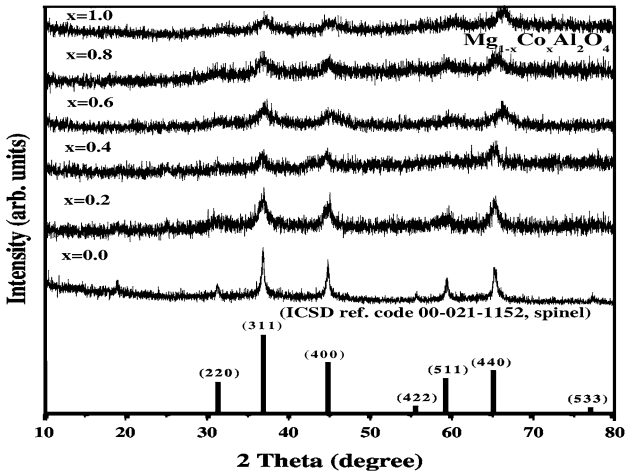

Fig. 2. Powder XRD patterns of $Mg_{1-x}Co_xAl_2O_4$ (x = 0.2, 0.4, 0.6, 0.8 and 1.0) spinel with the standard pattern (ICSD ref. code 00-021-1152, spinel).

d_{hkl} is the d-spacing value of the XRD pattern. It is noted that the lattice constant was increasing with Co^{2+} concentration in the $MgAl_2O_4$ spinel. The difference in the lattice constant was due to the difference in the ionic radii of the Co^{2+} ions (0.74 Å) and Mg^{2+} ions (0.65 Å). This increase in the lattice constant confirms the replacement of Mg^{2+} ions with Co^{2+} ions in the crystal lattice. The volume of the cell also increases with Co^{2+} concentration as it is the cube of the lattice constant. The x-ray density can be calculated from Eq. 3. The crystallite size of the synthesized sample is in the nano-domain range as can be seen in Table I.

Scanning Electron Microscopy Coupled with Energy Dispersive Spectroscopy

The morphology of the samples prepared at 800°C for 8 h was studied by SEM and the rmicrographs obtained are shown in Fig. 3. Figure 3a shows the pure $MgAl_2O_4$ sample and Fig. 3b shows the cobalt-doped derivative of $MgAl_2O_4$. Neither of the micrographs in Fig. 3 show any morphological variation which is evidence that incorporation of cobalt ions does not deform the cage structure of the spinel, since the surface morphology remains the same. Both the micrographs show large particle sizes. This is because magnesium aluminate is a very good candidate as a humidity sensor[3] due to its moisture-absorbing property. This is also the reason behind the large grain size which can be observed in the morphology of the samples in the SEM micrographs.

Energy Dispersive Spectroscopy

No structural deformation was obvious from the XRD data but there was no reasonable proof of whether or not cobalt replaced the sites. So, further verification of the sample was done with the support of EDS analysis which confirmed that the Co^{2+} ions had replaced the Mg^{2+} ions. Figure 3 shows the EDS

Table I. Calculated values of lattice constant (a), unit cell volume (V_{cell}), crystallite size (D) and density ($d_{x\text{-}ray}$) of $Mg_{1-x}Co_xAl_2O_4$ (x = 0.2, 0.4, 0.6, 0.8, 1.0) using XRD results

$Mg_{1-x}Co_xAl_2O_4$	0.0	0.2	0.4	0.6	0.8	1.0
a (Å)	8.080	8.080	8.068	8.057	8.047	8.988
V_{cell} (Å^3)	529	527	525	523	521	509
D_s (nm)	32	60.61	45.40	41.07	39.86	32.15
$d_{x\text{-}ray}$ (g cm^{-3})	3.57	3.75	3.94	4.14	4.33	4.61

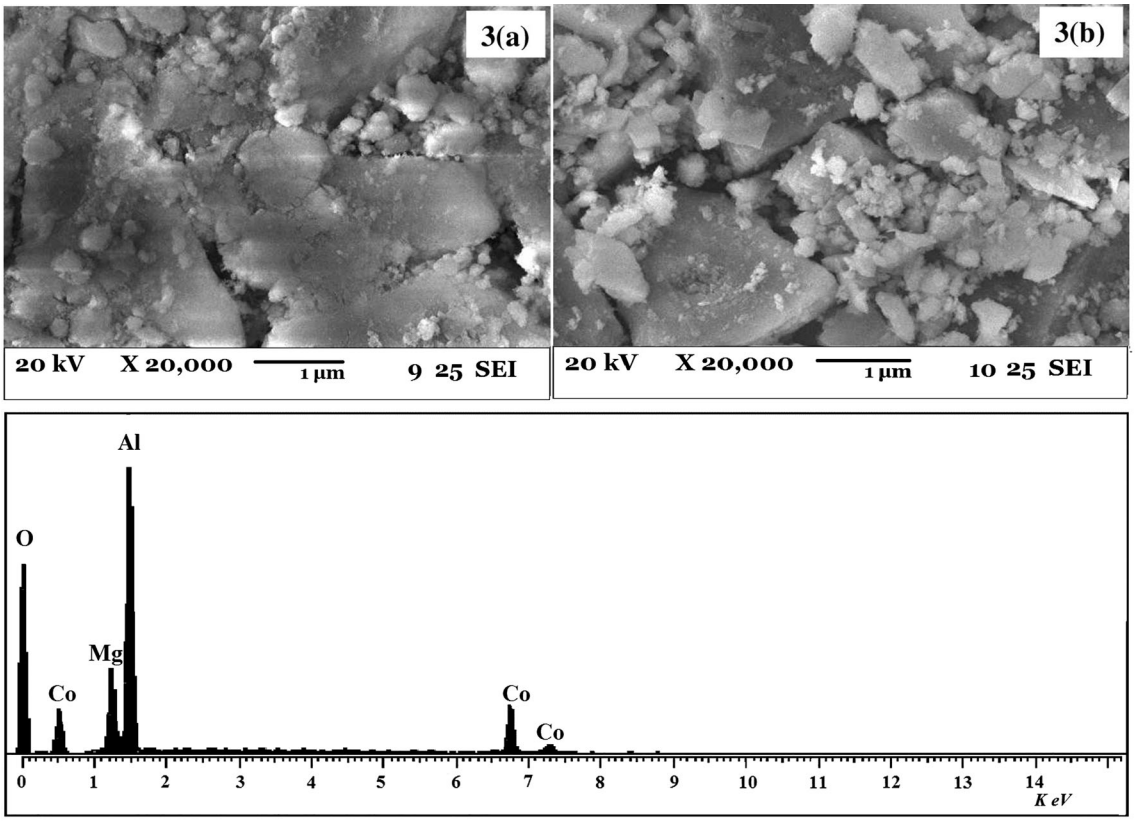

Fig. 3. SEM and EDS micrographs. (a) Pure MgAl2O4, (b) Mg0.2Co0.8Al2O4.

pattern of the $Mg_{0.2}Co_{0.8}Al_2O_4$ sample and it is very clear from the EDS pattern that the Mg^{2+} and Co^{2+} peaks are both visible, confirming the replacement of Mg^{2+} ions with Co^{2+} ions.

Fourier Transform Infrared Radiation

FTIR spectra recorded in the range (4000–400 cm^{-1}) of $MgAl_2O_4$ doped with Co^{2+} ions and heat-treated at 800°C for 8 h are shown in Fig. 4. Al-O bonds are usually seen in the lower range (1000–400 cm^{-1}), as in oxides of aluminum. Oxygen ions interact with aluminum oxides in several diverse ways. The stretching and bending of Al-O bonds show their peaks in the range 380–450 cm^{-1}, while hexa-coordinated cations (AlO_6), which construct the spinel, show their peaks in the 500–700 cm^{-1} range.[11] The peaks found around 410 cm^{-1} and 450 cm^{-1} indicate the formulation of Al-O bands, while the peaks of AlO_6 in $Mg_{1-x}Co_xAl_2O_4$ are at 662 cm^{-1} and 668 cm^{-1}. The peaks at around 1050 cm^{-1} and 1100 cm^{-1} are shoulder peaks of the O-H bending mode.[12] The bands seen around 3407 cm^{-1} and 3428 cm^{-1} correspond to the vibrations of the free OH group of water molecules and stretching surface vibrations.[13] The functional groups of $Mg_{1-x}Co_xAl_2O_4$ for different x contents evaluated from FTIR spectra are listed in Table II. The water peaks in the FTIR spectra also confirm the moisture absorption of the sample as seen in the SEM results. The peak at 2359 cm^{-1} shows a weak absorption peak of the NH_3 specimen. This peak can be representing some kind of undecomposed nitrate ions.

Ultra Violet-Visible Spectrum

UV–vis absorption spectrum, at room temperature, was recorded in the visible range (450–800 nm). The use of $MgAl_2O_4$ as a host lattice for cobalt-based phosphors has the advantage of the extraordinary chemical stability, elevated melting temperature (2135ºC)[2] and sufficient refractive index (1.723) of spinel. The absorption spectrum of pure $MgAl_2O_4$ is shown in Fig. 5. Two absorption edges can be seen in the pure spectrum, one at 230 nm[14] and the other at 268 nm. The band at 230 nm is attributed to anion vacancies incorporated by an electron, i.e. F^+-centers, while the band at 268 nm can be assigned to Mg^{2+} vacancies substituted by 2 electrons, i.e. F-centers. These vacancies are due to thermal treatment of the samples.

Co^{2+} ion is considered as a counter-partner of Cr^{3+} ions, so their energy level diagram is also considered to be the same with only a significant difference of ligand field strength of Cr^{3+} which is stronger than that of Co^{2+} ions. The energy level diagram of Co^{2+} ions in the tetrahedral symmetry site consists of a ground state ($^2A_{2g}$), two doublets (^2E) and ($^2T_1$) and also two quartets ($^4T_1$) and ($^4T_2$). The energy levels calculated in cm^{-1} and eV for $Mg_{1-x}Co_xAl_2O_4$ are tabulated in Table III.

Figure 6 shows UV–vis spectra of $Mg_{1-x}Co_xAl_2O_4$ (x = 0.2, 0.4, 0.6, 0.8 and 1.0). A strong absorption can be observed for the samples in the visible range (550–630 nm) which corresponds to absorption of yellow, orange and red colors. Thus, we expect that it will emit its complementary colors, violet, blue and green, having blue as its main wavelength. Cobalt (Co^{2+}) ions having $3d^7$ configurations can occupy tetrahedral and octahedral sites in spinel structures besides other possibilities—the vacancies caused by inversion effect due to heat treatment or charge transfer between ligand and metal ions. Three types of spin-allowed transitions $^4T_{1g}$

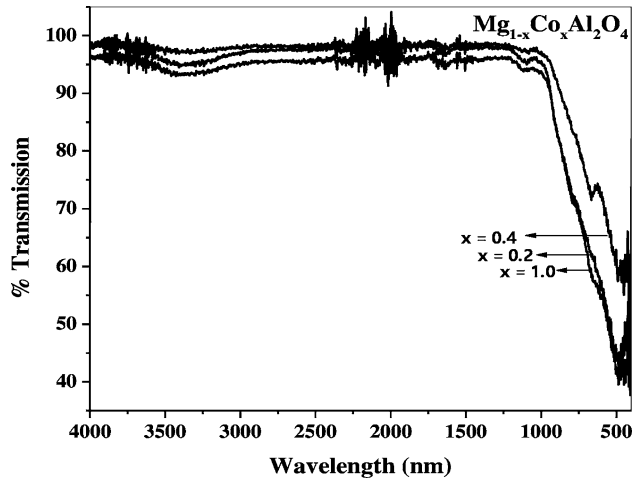

Fig. 4. FTIR spectra of $Mg_{1-x}Co_xAl_2O_4$ samples having x = 0.2, 0.6 and 1.0.

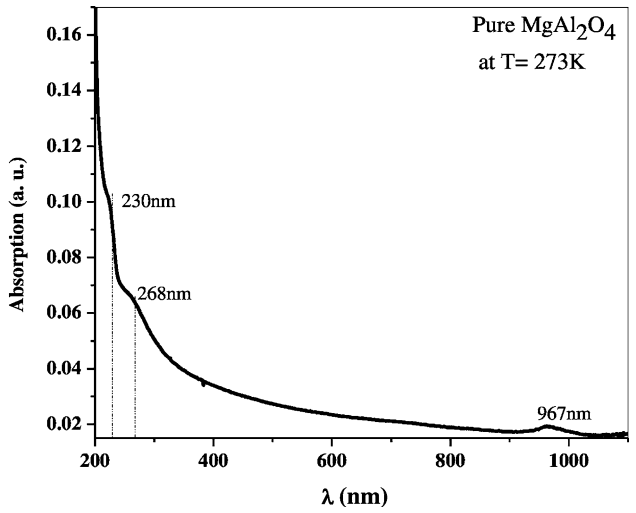

Fig. 5. Absorption spectrum of pure magnesium aluminate $MgAl_2O_4$.

Table III. Energy levels in cm^{-1} and eV for sample $Mg_{1-x}Co_xAl_2O_4$ (x = 0.2, 0.4, 0.6, 0.8, 1.0)

Energy level (nm)	Energy (cm^{-1})	Energy (eV)
540	18,519	2.296
580	17,241	2.137
628	15,924	1.974

Table II. Functional groups with different x contents for $Mg_{1-x}Co_xAl_2O_4$ (x = 0.2, 0.6, 1.0) as found by FTIR spectra

Chemical bond/functional groups for $Mg_{1-x}Co_xAl_2O_4$	Observed peaks for x = 0.2 (cm^{-1})	Observed peaks for x = 0.6 (cm^{-1})	Observed peaks for x = 1.0 (cm^{-1})
O-H (stretching)	3407	–	3428
N-H	–	–	2359
O-H (bending)	1076	–	–
Al-O-M	–	662	–
M-O (stretching peaks)	459, 414, 404	450, 418, 403	448, 418, 406

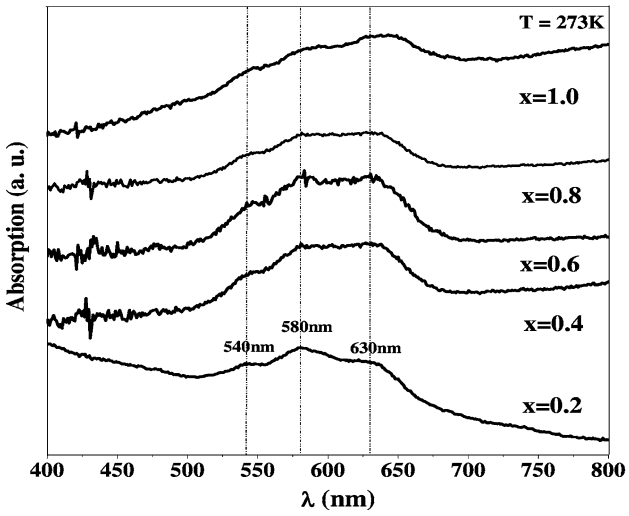

Fig. 6. UV–vis spectra of $Mg_{1-x}Co_xAl_2O_4$ sample having $x = 0.2$, 0.4, 0.6, 0.8 and 1.0.

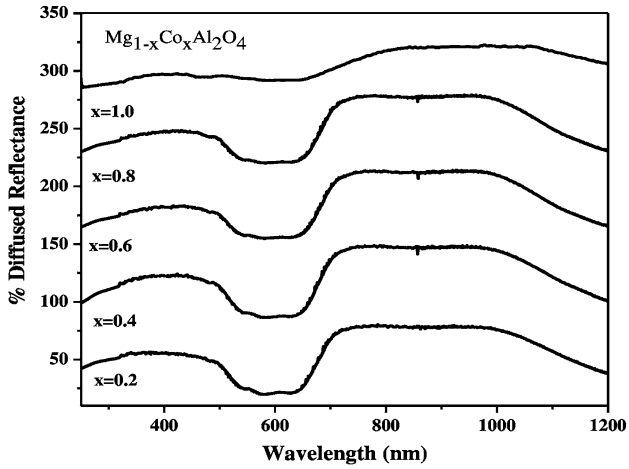

Fig. 7. DRS spectra of $Mg_{1-x}Co_xAl_2O_4$ samples having $x = 0.2$, 0.4, 0.6, 0.8 and 1.0.

(^4F) → $^4T_{2g}$, $^4A_{2g}$, $^4T_{1g}$ (4P) and two types of spin-forbidden transitions $^4T_{1g}$ (^4F) → $^2T_{2g}$ and $^2A_1$ can occur due to Co^{2+} ions.[15] A weak band at lower wavelengths (400–500 nm) is also seen, about which there is a conflict in ideas as to whether it is spin-forbidden or a transition due to the charge transfer of Co^{3+} at octahedral sites. The three main bands in Fig. 6 at 540 nm, 580 nm, and 630 nm, covering the visible regime of the electromagnetic spectrum, are assigned to spin-allowed transitions of Co^{2+} ions at tetrahedral sites of the spinel.

These results go well with the results obtained for Co^{2+} ions but having different host cage structures. Sales et al.[16] investigated these three bands at 510, 575 and 618 nm in the sample composition of $Al_{1.95}Co_{0.025}Ti_{0.025}$. SiO_2, calcinated at 995°C for 1 h. The bands were located at 544 nm, 580 nm, and 625 nm by Stangar et al.[17] while studying thin films of $CoAl_2O_4$ having a molar ratio 0.3 of Co/Al. Zayat and Levi[18] also observed the same three bands at 543 nm, 580 nm, and 630 nm in their $Co_{0.75}Al_{2.25}O_4$ powdered samples. Dondi et al.[19] reported the same kind of bands for AlTiO5 samples while investigating the cage with three different impurities (Co, Cr and Mn). De Souza et al.[20] observed bands at 550 nm, 580 nm and 620 nm while working with $Co_xZn_{1-x}Al_2O_4$ samples.

Besides strong bands, a weak band at a somewhat lower wavelength (473 nm) can also be seen, which is not prominent in a small content of cobalt, but becomes prominent with increasing cobalt concentration in the spinel cage. Zayat and levi[18] considered this band to be due to the spin-forbidden transition of Co^{2+} ions at octahedral sites, while Stangar et al.[17] illustrated this band due to Co^{3+} ions at octahedral sites. On the other hand, Kim et al.,[21] while studying the $Co_{3-x}Fe_xO_4$ structure, considered this band due to the charge transfer transition T_{2g} (Co^{3+}) → T_2 (Co^{2+}).

Diffused Reflectance Spectroscopy

Figure 7 shows the diffused reflectance of the samples recorded at room temperature in the range 250–1200 nm. A strong absorption region was observed for the samples at $x = 0.2$, 0.4, 0.6 and 0.8 in the range 550–630 nm, which corresponds to yellow to red color absorption and the emitting of its complementary colors, violet, blue and green. After further increasing the cobalt concentration in the spinel, the absorption wavelength decreases, which might be due to a concentration quenching effect. There is a possibility of three spin-allowed transitions $^4T_{1g}$ (^4F) → $^4T_{2g}$, $^4A_{2g}$ and $^4T_{1g}$ (4P) and two spin-forbidden transitions $^4T_{1g}$ (^4F) → $^2T_{2g}$ and $^2A_1$ which can occur due to the Co^{2+} ions.[22] In the DRS spectrum, the most intense band lies at 580 nm (17241 cm^{-1}) which is due to the spin-allowed transition $^4A_2$ (F) → $^4T_1$ (P). There are two shoulders of the band on both sides of 580-nm band, at 540 nm and 630 nm, corresponding to the energies 18,519 cm^{-1} and 15,924 cm^{-1}, respectively. Such a kind of splitting in the bands is caused by spin orbit coupling.[23]

Band Gap Studies

The optical band gap energy is evaluated from the diffused reflectance spectra, as shown in Fig. 8. From the slope of the graph of $[F(R)*h\nu]^2$ (eV) versus photon energy hc/λ (eV), the band gap of $MgAl_2O_4$ is found to be 5.36 eV and the absorption peak is expected to be at 231 nm. From Fig. 8, the optical band gap with different concentrations of cobalt was deduced to be between 5.31 eV and 2.32 eV for $x = 0.2$, 0.4, 0.6, 0.8 and 1.0. The absorption peak of $MgAl_2O_4$ should be in the ultraviolet region as indicated by its band gap energy of 5.36 eV, which can also be seen in Fig. 5. Then, the peaks in the visible region at 550 nm, 580 nm and 630 nm of the absorption spectra in Fig. 6 confirm that the band gap decreases by doping cobalt in $MgAl_2O_4$.

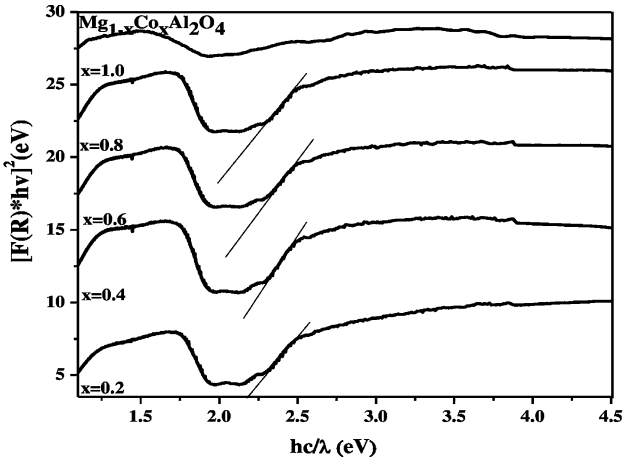

Fig. 8. Band gap spectra of $Mg_{1-x}Co_xAl_2O_4$ samples having x = 0.2, 0.4, 0.6, 0.8 and 1.0 calculated from diffused reflectance data.

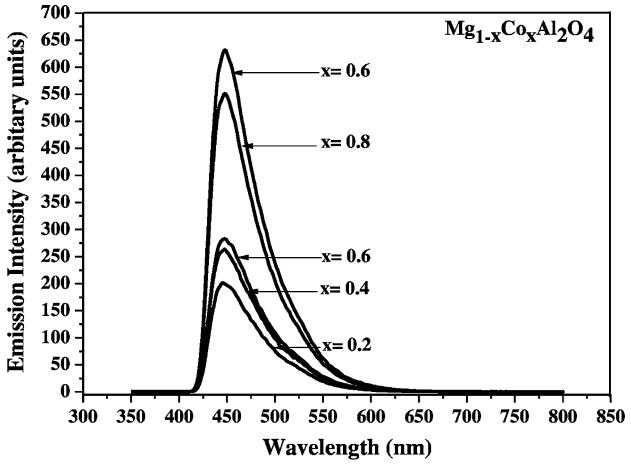

Fig. 9. Photoluminescence spectra of $Mg_{1-x}Co_xAl_2O_4$ samples having x = 0.2, 0.4, 0.6, 0.8 and 1.0.

Photoluminescence Studies

The PL spectra were recorded at room temperature with an excitation wavelength of 240 nm. Luminescence in $MgAl_2O_4$ samples can be created by three types of electron traps. The two types of hole traps can also be seen in the sample due to unknown intrinsic defects and due to Co^{2+} centers, which then recombine with the electrons. It may be caused by the vacancies created at the O^{-2} sites due to two different cation sites intermixing to emit luminescence. The electrons and holes created by ultraviolet excitation can be recombined by two different means. Intrinsic and Co^{2+} sites can be directly recombined with excited electrons to source fluorescence and the other, termed as phosphorescence, is caused by trapped electrons, which are activated thermally and recombine with some time lag.[12] The PL spectra of the samples of $Mg_{1-x}Co_xAl_2O_4$ (x = 0.2, 0.4, 0.6, 0.8 and 1.0) are shown in Fig. 9.

The intense emission peak observed at 449 nm is due to the relaxation of ions from the $4T_2(F)$ level to the ground state $4A_2(F)$. It is clearly observed from the spectra shown in Fig. 9 that, with the increase of cobalt concentration, there is no shift in band gap but the intensity is increased. The emission maxima can be seen for the sample having x = 0.6 and intensity decreases with further x-content. This decrease in intensity may be caused by the retardation effect of the cobalt nitrate ions on reaching a certain threshold value, called concentration quenching, as reported by Gluchoski et al.[23] The band gap and lattice constant of the sample varies due to variation of the Co^{2+}-O^{-2} distance which in turn shifts the luminescence band. The spectra showed no luminescence band shift which is consistent with the XRD results of the samples.

CONCLUSION

We successfully blended Co^{2+} ions retaining the spinel structure of $MgAl_2O_4$ by employing a co-precipitation method, as investigated by XRD data. EDS results witnessed the switching of Co^{2+} ions at T_d sites. Analysis of the SEM micrographs suggested that the morphology is not in accordance with the finer size of particles calculated by Scherrer's formula due to agglomeration of the particles. OH peaks obtained by FTIR analysis gave an indication of the moisture- absorbing property of the sample which caused the agglomeration. Pure magnesium aluminate showed its absorption peak at 231 nm but UV–vis and DRS showed the absorption peaks in the visible region because of Co^{2+} ion insertion, and there is a decrease in the band gap of pure magnesium aluminate from 5.31 eV without distortion of structure because of almost the same ionic radii of Mg^{2+} (0.65 Å) and Co^{2+} (0.67 Å). This reduces degradation of the luminescence as an irregular morphology is the drawback of the rare earth ions mostly used in phosphor technology. Decreases in particle size increases the surface area and defects which in turn increases the luminescent efficiency to make it very useful for photoconductivity, tunable laser operations and persistent phosphorescence. In the PL spectra, the variation was only observed in the intensity with an increase of Co^{2+} ions but no shift in the emission peak. This suggested that the emission was due to intrinsic defects in the $MgAl_2O_4$,[24] whereas the Co^{2+} ions only filled the vacancies.

ACKNOWLEDGEMENT

The services provided by Dr. Tajammul Hussain (Late) at National Center for Physics are strongly acknowledged by all the authors.

REFERENCES

1. J. Ahmed, M.Q. Awan, M.E. Mazhar, and M.N. Ashiq, *Phys. B* 406, 255 (2011).
2. V. Singh, R.P.S. Chakradhar, J.L. Rao, and D.K. Kim, *J. Solid State Chem.* 180, 2067 (2007).
3. I. Omkaram, G. Seeta Rama Raju, and S. Buddhudu, *J. Phys. Chem. Solids* 69, 2066 (2008).
4. H. Nakagawa, K. Ebisu, M. Zhang, and M. Kitaura, *J. Lumin.* 102–103, 590 (2003).
5. P.J. Deren, M. Malinowski, and W. Strek, *J. Lumin.* 68, 91 (1996).
6. A. Tomita, T. Sato, K. Tanaka, Y. Kawabe, M. Shirai, K. Tanaka, and E. Hanamura, *J. Lumin.* 109, 19 (2004).
7. J.F. Donegan, F.J. Bergin, and G.F. Imbush, *J. Lumin.* 31, 278 (1984).
8. M.M. Amini, M. Mirzaee, and N. Sepanj, *Mater. Res. Bull.* 42, 563 (2007).
9. M.J. Iqbal and B. Ismail, *J. Alloys Compd.* 504, 440 (2010).
10. E. Alagu Raja, S. Menon, B. Dhabekar, N.S. Rawat, and T.K. Gundu Rao, *J. Lumin.* 129, 829 (2009).
11. J. Guo, H. Lou, H. Zhao, Z. Wang, and X. Zheng, *Mater. Lett.* 58, 1922 (2004).
12. I. Omkaram, G.S.R. Raju, and S. Buddhudu, *J. Phys. Chem. Sol.* 69, 2066 (2008).
13. M.J. Iqbal and B. Kishwar, *Mater. Res. Bull.* 44, 763 (2009).
14. T.A. Bazilevskaya, V.T. Gritsyna, D.V. Orlinski, L.V. Udalova, and A.V. Voitsenya, *J. Nucl. Mater.* 253, 133 (1998).
15. R. Ianos, R. Lazău, and P. Barvinschi, *Adv. Powder Technol.* 22, 396 (2011).
16. I. Omkaram, and S. Buddhudu, *Opt. Mater.* 32, 8 (2009).
17. U.L. Stangar, B. Orel, and M. Krajnc, *J. Sol Gel Sci. Technol.* 26, 771 (2003).
18. M. Zayat and D. Levy, *Chem. Mater.* 12, 2765 (2000).
19. M. Dondi, T.S. Lyubenova, J.B. Carda, and M. Ocana, *J. Am. Ceram. Soc.* 92, 1979 (2009).
20. L.K.C. De Souza, J.R. Zamian, G.N.R. Filho, L.E.B. Soledade, I.M.G. Dos Santos, G. Souza, T. Scheller, R.S. Angelica, and C.E.F. Da Costa, *Dyes Pigments* 81, 190 (2009).
21. K.J. Kim, H.K. Kim, Y.R. Park, G.Y. Ahn, C.S. Kim, and J.Y. Park, *Hyp. Int.* 169, 1366 (2006).
22. A. Jouini, A. Yoshikwa, T. Fukuda, and G. Boulon, *J. Cryst. Growth* 293, 517 (2006).
23. P. Gluchoski, R. Pazik, and W.Strek Hreniak, *J. Phys. Chem.* 358, 53 (2009).
24. S.V. Motloung, F.B. Dejene, M.E. Sithole, L.F. Koao, O.M. Ntwaeaborwa, H.C. Swart, and T.E. Motaung, *J. Electron. Mater.* 45, 4796 (2016).